CHAPTER III

ONE-COLOR NONLINEAR WAVE PACKET INTERFEROMETRY

By employing a second pair of phase-locked pulses, nonlinear WPI is an extension of the single pulse-pair linear WPI experiments.[1,2] Originally put forth by Cina and Harris as a means to investigate superpositions of chiral amplitudes,[3] nonlinear WPI isolates the contributions to an electronic population linear in the four applied fields. These quadrilinear contributions to the population arise from the interference between the multiple nuclear wave packets excited by the incident pulses. As a form of phase-coherent, two-dimensional optical spectroscopy,[5] nonlinear WPI controls the wave-packet interference effects by shifting the two phase-locking angles. Combining population measurements taken with different values of the phase-locking angles, i.e. phase-cycling, isolates specific contributions to the population, and hence specific molecular responses.

In this chapter, we formulate the theory underlying one-color nonlinear WPI, in which each pulse-pair drives the same electronic transition. An isolated quadrilinear contribution then represents the sum of two wave-packet interference terms, each an overlap between a one-pulse wave-packet and a three-pulse wave packet. Similar to linear WPI measurements, the nonlinear WPI interferogram quantifies the interference between wave packets with respect to inter-pulse delay. For certain experimental

conditions, the information contained within the one-color nonlinear WPI interferogram is sufficient to perform molecular state reconstruction in a manner analogous to quantum state holography (QSH). [6,7]

Yet, unlike QSH, the one-pulse wave packet targeted for reconstruction in a nonlinear WPI experiment is not confined to the vertical transition point on the excited electronic surface. Instead, the target state undergoes a fixed period of field-free propagation in which it explores the underlying potential energy surface. And the three-pulse reference wave packets to be used for probing the target state are not limited to motion on a single energy shell, but can be manipulated to explore a (finite) volume of phase-space, thus increasing the possibilities for accurate reconstruction. Consequently, molecular state reconstruction using nonlinear WPI is capable of probing photoinduced nuclear dynamics leading to (excited-state) chemical reactions through reconstruction of the moving wave packets.

Theory

In one-color nonlinear WPI both pulse-pairs resonate with an electronic transition between the initial electronic level $|g\rangle$ and the final electronic level $|f\rangle$. In the absence of the fields, the molecular Hamiltonian is

$$H = |g\rangle H_g \langle g| + |f\rangle H_f \langle f| \tag{3.1}$$

where H_g and H_f are the nuclear Hamiltonians of g and f, respectively. The time-dependent interaction with the four fields is

$$V(t) = \sum_{j=1}^{4} V_j(t), \tag{3.2}$$

where for the jth field $(j = 1,2,3,4)$

$$V_j(t) = \hat{\ } \ \mathbf{E}_j(t). \tag{3.3}$$

The dipole moment operator

$$\hat{\ } = \ _{fg} |f\rangle\langle g| + \text{H.c.} \tag{3.4}$$

accounts for coupling between the electronic levels via the transition dipole moment vector $_{fg}$ and the jth electric field is defined as

$$\mathbf{E}_j(t) = \mathbf{e}_j A_j(t \quad t_j) \cos \ _j(t \quad t_j), \tag{3.5}$$

where $\mathbf{e}_j$ is the polarization vector, $A_j(t)$ is the temporal envelope, t_j is the arrival time of the pulse, and $_j(t)$ is the temporal phase. In the following, we specialize to the case $t_1 < t_2 < t_3 < t_4$, as shown in Fig. 3.1, and ignore effects due to pulse overlaps, though the latter can be important.[8,9] We denote interpulse delays as $t_{jk} = t_j \quad t_k$. For molecular state reconstruction, we hold the delay t_{43} constant while the remaining delays are varied.

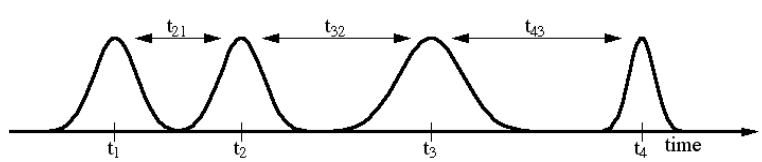

Fig. 3.1 The sequence of four pulses used in a nonlinear WPI experiment. The first two pulses comprise the first pulse-pair, while the last two pulse make up the second pulse-pair.

The first and second pulses constitute the first phase-locked pulse-pair, while the third and fourth pulse comprise the second phase-locked pulse-pair. Phase-locking each pulse-pair fixes the relative spectral-phase difference between the pulses at a specific locking frequency. We define the Fourier component of the jth pulse at a frequency as

$$_{j}(\ )e^{\ i\ _{j}(\ )+i\ \ t_{j}} = e^{i\ \ t_{j}}\ \ dte^{i\ \ t}A(t)\cos\ \ _{j}(t), \tag{3.6}$$

where $_{j}(\ )$ is the spectral amplitude and $_{j}(\ )\ \ t_{j}$ is the spectral phase. Phase-locking the first pulse-pair at the (optical) locking-frequency $_{L}$ introduce the phase-locking angle

$$= \ _{2}(\ _{L})\ \ _{1}(\ _{L})\ \ _{L}t_{21}. \tag{3.7}$$

Similarly, the phase-locking angle of the second pulse-pair is defined at the locking-frequency $_{L}$ as

$$= \ _{4}(\ _{L})\ \ _{3}(\ _{L})\ \ _{L}t_{43}. \tag{3.8}$$

Differences between the spectral phases of other members in the pulse sequence are not considered to be controlled, but are expected to fluctuate between measurements. Appendix C discusses the role these phase fluctuations play in signal averaging.

The molecular amplitude following the action of the pulse sequence is determined by solving Schrödinger's equation

$$i\frac{|\ \ (t)\rangle}{t} = H(t)|\ \ (t)\rangle, \tag{3.9}$$

where $H(t) = H + V(t)$ is the time-dependent Hamiltonian, $\left| \quad (t) \right\rangle$ is the molecular probability amplitude, and we have set $\hbar = 1$. Well before the arrival of the pulses the molecular state is taken as

$$\left| \quad (t << t_1) \right\rangle = |g\rangle e^{\ iH_g(t \quad t_3)} \left| \quad {}_g \right\rangle, \tag{3.10}$$

i.e. a nuclear eigenstate $\left| \quad {}_g \right\rangle$ of the ground electronic level. We switch to the interaction picture, defined by

$$\left| \tilde{\ } (t) \right\rangle = e^{iHt} \left| \quad (t) \right\rangle, \tag{3.11}$$

and solve the corresponding equation of motion

$$i \frac{\left| \tilde{\ } (t) \right\rangle}{t} = \tilde{V}(t) \left| \tilde{\ } (t) \right\rangle \tag{3.12}$$

driven by the interaction operator

$$\tilde{V}(t) = e^{iHt} V(t) e^{\ iHt}. \tag{3.13}$$

Formal integration of Eq. (3.12) yields

$$\left| \tilde{\ } (t) \right\rangle = \left| \tilde{\ } (t_0) \right\rangle \quad i \int_{t_0}^{t} d \ \tilde{V}(\ ) \left| \tilde{\ } (t) \right\rangle, \tag{3.14}$$

where the initial time t_0 is before the interaction turns on and the final time *t* is well after the last pulse acts. Taking the weak-field limit, we expand the solution (3.14) out to third order in the interaction $\tilde{V}(t)$ and project out the amplitude in the *f* electronic level to find

$$\left\langle f \right| \tilde{\ } (t) \left\rangle = \right) \quad i \quad d \ \langle f | \tilde{V}(\ ) | g \rangle \qquad d \qquad d \quad \langle f | \tilde{V}(\ ) \tilde{V}(\ ) | g \rangle \tag{3.15}$$

$$+i \quad d \quad d \quad d \quad \langle f|\tilde{V}(\ )\tilde{V}(\ )\tilde{V}(\ )|g\rangle(e^{iH_g t_3}|)_g\rangle.$$

In deriving Eq. (3.15), we have substituted the initial condition from Eq. (3.10); the zeroth-order term vanishes as the g and f electronic levels are orthogonal. To obtain explicit expression for the nuclear wave packets contributing to the f-state amplitude we evaluate each remaining interaction in Eq. (3.15).

First-order interactions leading to f-state amplitude are written as

$$i \quad d \ \langle f|\tilde{V}_j(\ )|g\rangle = i \quad d \ A_j(\quad t_j)\cos \quad {}_j(\quad t_j)e^{iH_f}\left(\ {}_{fg}\ \mathbf{e}\right)_j e^{\ iH_g} \tag{3.16}$$

$$= e^{iH_f t_j} P_j^{fg} e^{\ iH_g t_j},$$

where the pulse propagator

$$P_j^{fg} = i \quad d \ A_j(\ )\cos \quad {}_j(\ )e^{iH_f}\left(\ {}_{fg}\ \mathbf{e}\right)_j e^{\ iH_g} \tag{3.17}$$

describes the transfer of nuclear amplitude from g to f via the jth pulse. The reverse transition is given by

$$P_j^{gf} = \quad P_j^{fg\dagger}. \tag{3.18}$$

One benefit to using the pulse propagator is that electronic excitation and the changes in the nuclear wave packet due to pulse shaping are incorporated into this instantaneous operator. It is easily seen that the pulse propagator is proportional to the spectrum; using the nuclear eigenstates of g and f, we have

$$\langle\ {}_f|P_j^{fg}|\ {}_g\rangle = i\langle\ {}_f|\quad \mathbf{e}_j|\ {}_g\rangle \quad d \ e^{i\left(E_f(\ {}_f)\ E_g(\ {}_g)\right)} A_j(\ )\cos \quad {}_j(\ ) \tag{3.19}$$

$$= i\langle \quad {}_f \big| \quad \mathbf{e}_j \big| \quad {}_g \rangle \quad {}_j \Big(E_f \big(\quad {}_f \big) \quad E_g \big(\quad {}_g \big) \Big) e^{\quad i \left(E_f \left(\quad {}_f \right) \quad E_g \left(\quad {}_g \right) \right)} .$$

As should be expected, for the pulse propagator to transfer amplitude between electronic levels, the pulse must have bandwidth at the resonance frequency $E_f\big(\quad {}_f \big) \quad E_g\big(\quad {}_g \big)$. In the case of a one-color experiment, all four pulses drive $f \qquad g$.

Second-order contributions are analyzed in a similar manner. However, a two pulse transition involves the $g \qquad f \qquad g$ sequence of electronic excitation; therefore, no *f*-state amplitude is expected from the second integral operator in Eq. (3.15).

Third-order contributions to the *f*-state amplitude result from the $f \qquad g \qquad f \qquad g$ electronic-excitation sequence and may arise from a single pulse driving three-photon transitions, as well as combinations of pulses. For a single pulse, we write the third-order interaction as

$$i \quad d \qquad d \qquad d \quad \langle f | \tilde{V}_j(\quad) \tilde{V}_j(\quad) \tilde{V}_j(\quad) | g \rangle = e^{iH_f t_j} R_j^{fg} e^{\quad iH_g t_j} , \tag{3.20}$$

where

$$R_j^{fg} = i \quad d \; e^{iH_f} \quad {}_{fg} \; \mathbf{e}_j A_j(\quad) \cos \quad {}_j(\quad) e^{\quad iH_g} \tag{3.21}$$

$$\Big(d \quad e^{iH_g} \quad {}_{fg} \; \mathbf{e}_j A_j(\quad) \cos \quad {}_j(\quad) e^{\quad iH_f}$$

$$\Big(d \quad e^{iH_f} \quad {}_{fg} \; \mathbf{e}_j A_j(\quad) \cos \quad {}_j(\quad) e^{\quad iH_g}$$

describes the three-photon excitation sequence. When two pulses contribute to the preparation of the *f*-state amplitude, with the first acting to second order, we write

$$i \quad d \quad d \quad d \quad \langle f|\tilde{V}_j(\ )\tilde{V}_k(\ )\tilde{V}_k(\ )|g\rangle = e^{iH_f t_j} P_j^{fg} e^{\ iH_g t_{jk}} Q_k^{fg} e^{\ iH_g t_k}, \tag{3.22}$$

where P_j^{fg} was defined in Eq. (3.17) and

$$Q_k^{fg} = \quad d \ e^{iH_g} \quad {}_{fg} \ \mathbf{e}_k A_k(\ )\cos \ {}_k(\ ) e^{\ iH_f} \tag{3.23}$$

$$\Big(d \ e^{iH_f} \quad {}_{fg} \ \mathbf{e}_k A_k(\ )\cos \ {}_k(\ ) e^{\ iH_g}$$

describes the two-photon transition sequence $g \quad f \quad g$. In going to the RHS of Eq. (3.17), we have extended the upper limit of integration over to infinity as the pulses *j* and *k* are assumed to not overlap. A variation on the former interaction, in which the first pulse enters linearly and the second pulse acts to second order, is also possible. In that case,

$$i \quad d \quad d \quad d \quad \langle f|\tilde{V}_j(\ )\tilde{V}_j(\ )\tilde{V}_k(\ )|g\rangle = e^{iH_f t_j} Q_j^{gf} e^{\ iH_g t_{jk}} P_k^{fg} e^{\ iH_g t_j}, \tag{3.24}$$

where Q_j^{gf} is analogous to Eq. (3.23), but with the role of the Hamiltonians reversed. Finally, and of specific interest in a nonlinear WPI experiment, there are contributions to the *f*-state amplitude which results from the action of all three pulses, i.e.

$$i \quad d \quad d \quad d \quad \langle f|\tilde{V}_j(\ )\tilde{V}_k(\ )\tilde{V}_l(\ )|g\rangle \tag{3.25}$$

$$= e^{iH_f t_j} P_j^{fg} e^{\ iH_g t_{jk}} P_k^{gf} e^{\ iH_f t_{kl}} P_l^{fg} e^{\ iH_g t_l} \qquad (j \quad k \quad l).$$

In going to the last line of Eq. (3.25), we have made use of the fact that we are neglecting effects arising from pulse overlap, permitting the upper limit of integration to be extended

to infinity for each integral. Then the triple integral is separated into three single integrals and our definition of the pulse propagator in Eq. (3.17) is used.

For the *f*-state amplitude, we retain only those terms above which satisfy the time-ordering $t_1 < t_2 < t_3 < t_4$. Then each prepared nuclear wave packet is denoted according to the pulses that prepare it. The *f*-state nuclear amplitude in the interaction picture at a time well after the action of the last pulse is written as

$$\begin{aligned}\left\langle f\right|\tilde{\ }\left(t >> t_4\right)\rangle = e^{iH_f t_4}\ & \left|(1)_f\right\rangle + \left|(2)_f\right\rangle e^{\ i} + \left|(3)_f\right\rangle + \left|(4)_f\right\rangle e^{\ i} \\ & + \left|(111)_f\right\rangle + \left|(211)_f\right\rangle e^{\ i} + \left|(311)_f\right\rangle + \left|(411)_f\right\rangle e^{\ i} \\ & + \left|(221)_f\right\rangle + \left|(222)_f\right\rangle e^{\ i} + \left|(322)_f\right\rangle + \left|(422)_f\right\rangle e^{\ i} \\ & + \left|(331)_f\right\rangle + \left|(332)_f\right\rangle e^{\ i} + \left|(333)_f\right\rangle + \left|(433)_f\right\rangle e^{\ i} \\ & + \left|(441)_f\right\rangle + \left|(442)_f\right\rangle e^{\ i} + \left|(443)_f\right\rangle + \left|(444)_f\right\rangle e^{\ i} \\ & + \left|(321)_f\right\rangle e^{i} + \left|(421)_f\right\rangle e^{i(\quad)} + \left|(431)_f\right\rangle e^{\ i} + \left|(432)_f\right\rangle e^{\ i(\ +\ )}\ .\end{aligned} \tag{3.26}$$

Our abbreviated notation highlights the interaction(s) leading to preparation of the 24 wave packets. For instance, those four wave packets linear in one of the pulses are defined as

$$\left|(1)_f\right\rangle = e^{\ iH_f t_{41}} P_1^{fg} e^{iH_g t_{31}} \left|\ _g\right\rangle \tag{3.27}$$

$$\left|(2)_f\right\rangle = e^{\ iH_f t_{42}} P_2^{fg} e^{iH_g t_{32}} \left|\ _g\right\rangle \tag{3.28}$$

$$\left|(3)_f\right\rangle = e^{\ iH_f t_{43}} P_3^{fg} \left|\ _g\right\rangle \tag{3.29}$$

$$\left|(4)_f\right\rangle = P_4^{fg} e^{\ iH_g t_{43}} \left|\ \ _g\right\rangle, \tag{3.30}$$

while the 4 wave packets linear in three pulses are

$$\left|(421)_f\right\rangle = P_4^{fg} e^{\ iH_g t_{42}} P_2^{gf} e^{\ iH_f t_{21}} P_1^{fg} e^{iH_g t_{31}} \left|\ \ _g\right\rangle. \tag{3.31}$$

$$\left|(321)_f\right\rangle = e^{\ iH_f t_{43}} P_3^{fg} e^{\ iH_g t_{32}} P_2^{gf} e^{\ iH_f t_{21}} P_1^{fg} e^{iH_g t_{31}} \left|\ \ _g\right\rangle. \tag{3.32}$$

$$\left|(431)_f\right\rangle = P_4^{fg} e^{\ iH_g t_{43}} P_3^{gf} e^{\ iH_f t_{31}} P_1^{fg} e^{iH_g t_{31}} \left|\ \ _g\right\rangle. \tag{3.33}$$

$$\left|(432)_f\right\rangle = P_4^{fg} e^{\ iH_g t_{43}} P_3^{gf} e^{\ iH_f t_{32}} P_2^{fg} e^{iH_g t_{32}} \left|\ \ _g\right\rangle. \tag{3.34}$$

Illustrations of the dynamics which lead to preparation of the 8 wave packets above are shown in Figs. 3.2 – 3.5. Explicit expression for the remaining wave packets are found in Appendix B. Note that the 24 wave packets on the RHS of Eq. (3.26) are defined with both pulse-pairs in-phase, i.e. both phase-locking angles set to 0. The dependence of each wave packet on the phase-locking angles is explicated by the accompanying phase factors. These phase factors arise from shits in the spectral phase of the second or fourth pulse, or both. The two-photon pulse propagator Q_j^{ba} is independent of shifts in spectral phase, while the one- and three-photon pulse propagators, P_j^{ba} and R_j^{ba}, are not. For $j = 2$ or 4, the latter operators acquire a phase of either $e^{\ i}$ or $e^{\ i}$, respectively, assuming $b \quad a$ is an upward transition. Otherwise, the conjugate relations apply; see Eq. (3.18). Note also that the state (3.26) has been back-propagated in anticipation of transforming the amplitude back to the Schrödinger picture.

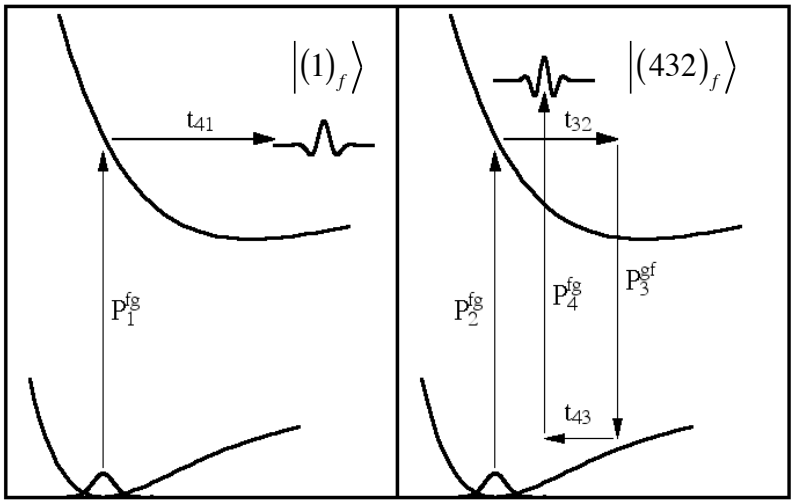

Fig. 3.2 The wave packets $|(1)_f\rangle$ and $|(432)_f\rangle$ in a one-color experiment.

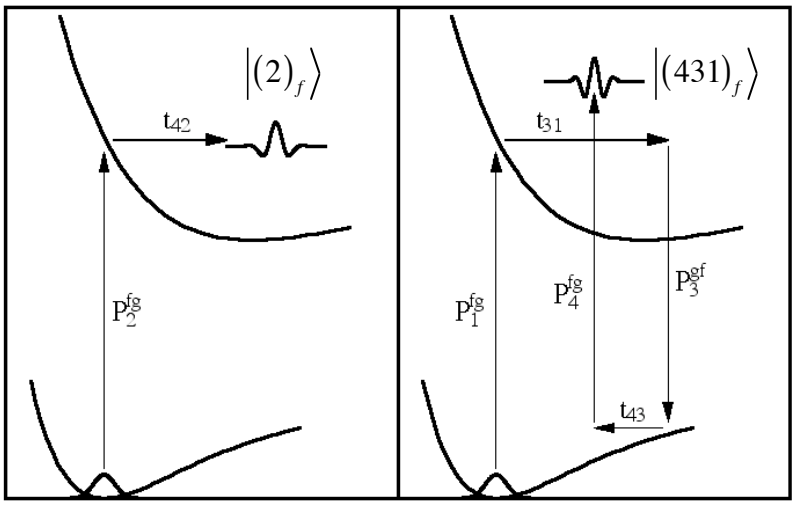

Fig. 3.3 The wave packets $|(2)_f\rangle$ and $|(431)_f\rangle$ in a one-color experiment.

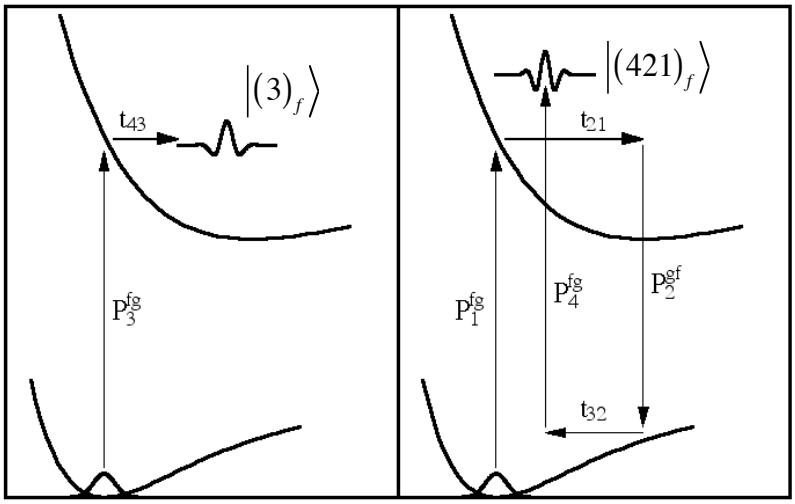

Fig. 3.4 The wave packets $|(3)_f\rangle$ and $|(421)_f\rangle$ in a one-color experiment.

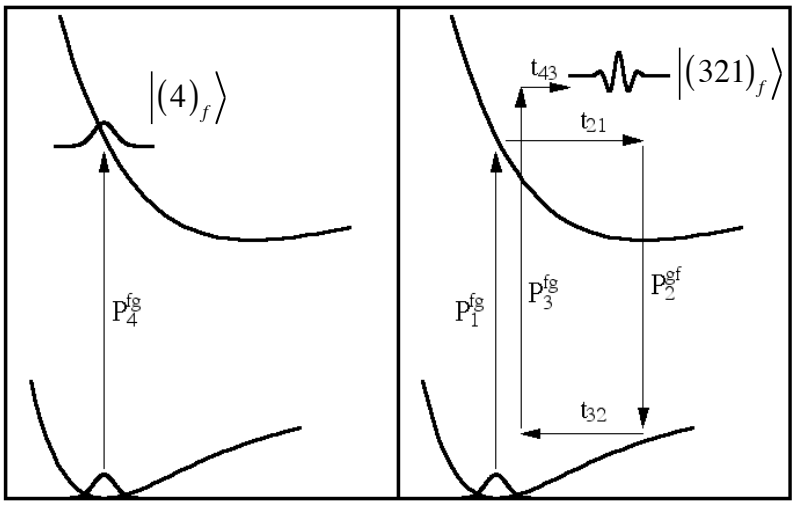

Fig. 3.5 The wave packets $|(4)_f\rangle$ and $|(321)_f\rangle$ in a one-color experiment.

Using the inverse of Eq. (3.11) and our expression for the *f*-state amplitude in Eq. (3.26), we transform from the interaction picture to the Schrödinger picture and obtain for the state long after the action of the last pulse

$$\begin{aligned}\langle f| \quad (t >> t_4)\rangle = e^{\ iH_f(t\ \ t_4)}\ & |(1)_f\rangle + |(2)_f\rangle e^{\ i\ \ } + |(3)_f\rangle + |(4)_f\rangle e^{\ i\ \ } \\ & + |(111)_f\rangle + |(211)_f\rangle e^{\ i\ \ } + |(311)_f\rangle + |(411)_f\rangle e^{\ i\ \ } \\ & + |(221)_f\rangle + |(222)_f\rangle e^{\ i\ \ } + |(322)_f\rangle + |(422)_f\rangle e^{\ i\ \ } \\ & + |(331)_f\rangle + |(332)_f\rangle e^{\ i\ \ } + |(333)_f\rangle + |(433)_f\rangle e^{\ i\ \ } \\ & + |(441)_f\rangle + |(442)_f\rangle e^{\ i\ \ } + |(443)_f\rangle + |(444)_f\rangle e^{\ i\ \ } \\ & + |(321)_f\rangle e^{i\ \ } + |(421)_f\rangle e^{i(\quad)} \\ & + |(431)_f\rangle e^{\ i\ \ } + |(432)_f\rangle e^{\ i(\ +\ )}\ .\end{aligned} \tag{3.35}$$

The corresponding population of the electronic level is

$$P_f(\ ,\ \ ) = |\langle f| \quad (t)\rangle|^2 . \tag{3.36}$$

Inserting Eq. (3.35) into (3.36) yields an expression for the *f*-state population, valid for any given laser short. However, many contributions to the *f*-state population depend on the spectral-phase difference between pairs of *non-phase-locked* pulses. It is expected that in a nonlinear WPI experiment population measurements will necessarily be averaged over a sequence of many laser shorts so as to reduce the signal-to-noise level, and that during the averaging process the spectral-phase difference between pairs of non-phase-locked pulses will fluctuate uniformly between values of 0 and 2 .

Accordingly, those contributions to the population which depend on the spectral phase difference between non-phase-locked pulses will vanish. In Appendix C, we give the expression for the single-shot population and discuss which contributions should vanish on signal averaging.

Implicitly performing the signal averaging procedure by neglecting those shot-to-shot contributions to the population which depend on the spectral-phase difference of non-phase-locked pulses (see Appendix C), we express the *f*-state population up to fourth order in the applied field amplitudes is

$$P_f(\ ,\ ) = \sum_{m=-1}^{1}\sum_{n=-1}^{1} p_{mn} e^{i(m\ +n\ )} \tag{3.37}$$

with the (Fourier) coefficients defined as

$$\begin{aligned} p_{0,0} = {} & \langle (1)_f | (1)_f \rangle + \langle (2)_f | (2)_f \rangle + \langle (3)_f | (3)_f \rangle + \langle (4)_f | (4)_f \rangle \\ & + \langle (111)_f | (1)_f \rangle + \langle (211)_f | (2)_f \rangle + \langle (311)_f | (3)_f \rangle + \langle (411)_f | (4)_f \rangle \\ & + \langle (221)_f | (1)_f \rangle + \langle (222)_f | (2)_f \rangle + \langle (322)_f | (3)_f \rangle + \langle (422)_f | (4)_f \rangle \\ & + \langle (331)_f | (1)_f \rangle + \langle (332)_f | (2)_f \rangle + \langle (333)_f | (3)_f \rangle + \langle (433)_f | (4)_f \rangle \\ & + \langle (333)_f | (3)_f \rangle + \langle (433)_f | (4)_f \rangle + \langle (441)_f | (1)_f \rangle + \langle (442)_f | (2)_f \rangle \\ & + \langle (443)_f | (3)_f \rangle + \langle (444)_f | (4)_f \rangle + \text{c.c.} \end{aligned} \tag{3.38}$$

$$\begin{aligned} p_{1,0} = {} & \langle (2)_f | (1)_f \rangle + \langle (2)_f | (111)_f \rangle + \langle (211)_f | (1)_f \rangle + \langle (2)_f | (221)_f \rangle \\ & + \langle (222)_f | (1)_f \rangle + \langle (2)_f | (331)_f \rangle + \langle (332)_f | (1)_f \rangle + \langle (2)_f | (441)_f \rangle \end{aligned} \tag{3.39}$$

$$+\left\langle (442)_f \middle| (1)_f \right\rangle + \left\langle (1)_f \middle| (321)_f \right\rangle + \left\langle (321)_f \middle| (3)_f \right\rangle + \left\langle (421)_f \middle| 4 \right\rangle$$

$$p_{0,1} = \left\langle (4)_f \middle| (3)_f \right\rangle + \left\langle (4)_f \middle| (311)_f \right\rangle + \left\langle (411)_f \middle| (3)_f \right\rangle + \left\langle (4)_f \middle| (322)_f \right\rangle \tag{3.40}$$

$$+\left\langle (422)_f \middle| (3)_f \right\rangle + \left\langle (4)_f \middle| (333)_f \right\rangle + \left\langle (433)_f \middle| (3)_f \right\rangle + \left\langle (4)_f \middle| (443)_f \right\rangle$$

$$+\left\langle (444)_f \middle| (3)_f \right\rangle + \left\langle (431)_f \middle| (1)_f \right\rangle + \left\langle (431)_f \middle| (1)_f \right\rangle + \left\langle (432)_f \middle| (2)_f \right\rangle$$

$$p_{1,1} = \left\langle (432)_f \middle| (1)_f \right\rangle + \left\langle (4)_f \middle| (321)_f \right\rangle \tag{3.41}$$

and

$$p_{1,1} = \left\langle (431)_f \middle| (2) \right\rangle + \left\langle (421)_f \middle| (3) \right\rangle \tag{3.42}$$

with the condition that $p_{m,n} = p_{m,n}$.

The form of Eq. (3.37) is suggestive of a two-dimensional Fourier series in the variables and . In general, any function $f(x,y)$ periodic in both x and y, having periods $2T$ and $2T$, respectively, can be expressed as a two-dimensional Fourier series[10]

$$f(x,y) = \underset{m=}{} \underset{n=}{} c_{mn} e^{i(mx+ny)} \tag{3.43}$$

with the Fourier coefficients defined by

$$c_{mn} = \frac{1}{4TT} \int_T^T dx \int_T^T dy\, f(x,y) e^{i(mx/T+ny/T)} . \tag{3.44}$$

The population expression of Eq. (3.37) is just such a function with periods $2T = 2T = 2$. The inversion formula given by Eq. (3.44) is therefore applicable for

determining contributions to the population with a specific phase signature. The corresponding expression is

$$p_{mn} = \frac{1}{4^{2}} \quad d \quad d \quad P_f(\quad , \quad) e^{i(m \quad + n \quad)} . \tag{3.45}$$

Though formally exact, Eq. (3.45) is considered impractical for experimental determination of the quadrilinear interference terms $p_{1,1}$ and $p_{1,1}$, as it would require continuous sampling of the *f*-state population with respect to both phase-locking angles. Realistically, we may assume the *f*-state population to be sampled at evenly spaced values of the phase-locking angles with an interval between values (we consider the sampling interval of both phase-locking angles to be the same.) The possible values of and are then integer multiples of , i.e.

$$_{j} = j \quad \text{and} \quad _{k} = k \quad . \tag{3.46}$$

for $j,k = 0,1,2,...K \quad 1$. We assume the integer K is such that $_{K} = 2$, which is equivalent to assuming the sampling interval is a rational fraction of the periods, $= 2 \quad / K$. We replace both integrals in Eq. (3.45) by a finite sum over the evenly sampled data, yielding

$$p_{mn} = \frac{2 \quad K \quad 1 K \quad 1}{4^{2}} \sum_{j=0 \; k=0} P_f\left(\quad _{j}, \quad _{k} \right) e^{i\left(m \quad _{j} + n \quad _{k}\right)} . \tag{3.47}$$

Equation (3.47) is an analytic expression for isolating any of the Fourier coefficients of the population. From our perturbative analysis of the population, we conclude that there are nine independent quantities to the population, and as such, we expect a total of nine population measurements to be necessary, i.e. $K^2 = 9$. Equation (3.47) is then written as

$$p_{mn} = \frac{1}{9} \sum_{j=0}^{2} \sum_{k=0}^{2} P_f(j\ \ ,k\ \ ) e^{\ i(mj+nk)} \tag{3.48}$$

with $\ \ = 2\ \ / 3$. The quadrilinear interference term $p_{\ 1,1}$ is then given by

$$\begin{aligned} p_{\ 1,1} = \frac{1}{9}\Big(& P_f(0,0) + P_f(0,\ \ )e^{\ i\ \ } + P_f(0,2\ \ )e^{i} \\ & + P_f(\ \ ,0)e^{i\ \ } + P_f(\ \ ,\ \ ) + P_f(\ \ ,2\ \ )e^{\ i} \\ & + P_f(2\ \ ,0)e^{\ i\ \ } + P_f(2\ \ ,\ \ )e^{i\ \ } + P_f(2\ \ ,2\ \ )\Big), \end{aligned} \tag{3.49}$$

as can be verified by using Eq. (3.37). Similarly, the remaining quadrilinear interference is given by

$$\begin{aligned} p_{1,1} = \frac{1}{9}\Big(& P_f(0,0) + P_f(0,\ \ )e^{\ i\ \ } + P_f(0,2\ \ )e^{i} \\ & + P_f(\ \ ,0)e^{\ i\ \ } + P_f(\ \ ,\ \ )e^{i\ \ } + P_f(\ \ ,2\ \ ) \\ & + P_f(2\ \ ,0)e^{i\ \ } + P_f(2\ \ ,\ \ ) + P_f(2\ \ ,2\ \ )e^{\ i\ \ }\Big). \end{aligned} \tag{3.50}$$

The combination of measurements necessary for isolating the remaining Fourier coefficients can also be determined from Eq. (3.48). When all five (unique) Fourier coefficients are recovered, the population of Eq. (3.37) can be formed. When fewer than nine measurements are used aliasing may corrupt isolation of the Fourier coefficients.[11] Also, if the perturbative expression for the population should fail to account for higher-order terms in the phase-locking angles, e.g., $p_{2,0}e^{\ i2}$, then more than nine measurements will be necessary to isolate a given coefficient. Those higher-order terms (at least at sixth-order in the applied field amplitudes) are expected to be much smaller than the second- and fourth-order terms of interest here.

Molecular State Reconstruction

In general, the quadrilinear contribution to the population given by Eq. (3.42) and isolated according to Eq. (3.49) represents a sum the overlaps $\left\langle (431)_f \middle| (2)_f \right\rangle$ and $\left\langle (421)_f \middle| (3)_f \right\rangle$. But mixing of these two wave-packet interferences can be minimized when the system's dynamics and the spectral bandwidth of the pulses are taken into account. As noted first by Cina,[4] the differences between the one-pulse wave packets $\left| (2)_f \right\rangle$ and $\left| (3)_f \right\rangle$ are due mostly to a longer period of propagation in the excited electronic level for the former (the differences between the second and third pulses being assumed small). If the delay t_{32} is chosen sufficiently large, the wave packet $\left| (2)_f \right\rangle$ will explore regions of the excited surface far from the Franck-Condon point, where the electronic difference potential is red-shifted relative to the absorption maximum. In this case, substantial overlap between $\left| (2)_f \right\rangle$ and $\left| (431)_f \right\rangle$ can only occur if the spectral bandwidths of the third and fourth pulses encompass those (red-shifted) $f \quad g$ transition frequencies; otherwise, the overlap is diminished. The extent to which the relevant resonance frequencies are red-shifted is determined by the electronic difference potential and hence the limitations on bandwidth necessary to minimize mixing of the overlaps varies from molecule to molecule.

In contrast, the one-pulse wave packet $\left| (3)_f \right\rangle$ propagates for a delay t_{43} which is varied independently of t_{32}. And the three-pulse wave packet $\left| (421)_f \right\rangle$ is not subjected to

spectral discrimination arising from the bandwidth of the second pulse-pair; it propagates on the g surface during the presumedly long delay t_{32}. Therefore, while spectral bandwidth may diminish one of the overlaps, the other is not (necessarily) minimized and parts of the nonlinear WPI interferogram will represent a single overlap.

Let us assume mixing of the overlaps in Eq. (3.42) have been minimized based on bandwidth considerations and that a collection of M signal measurements

$$z_m = \left\langle (421)_f \middle| (3)_f \right\rangle, \tag{3.51}$$

where $m = (t_{21}, t_{32})$ is an index of the delay times used, are measured according to Eq. (3.49). We recast the wave-packet interference data as

$$z_m = \left\langle \mathrm{ref}_{421}\left(\quad {}_g \right) \middle| \mathrm{tar}_3\left(\quad {}_g \right) \right\rangle, \tag{3.52}$$

where the target state is defined as

$$\left| \mathrm{tar}_3\left(\quad {}_g \right) \right\rangle = e^{i\left({}_3\left(\quad {}_L \right) + i \quad {}_L t_{43} \right)} e^{\ iH_f t_{43}} P_3^{fg} \left| \quad {}_g \right\rangle \tag{3.53}$$

and represents preparation of a nuclear wave packet on the f surface by the third pulse that propagates for the fixed delay t_{43}. The reference state in Eq. (3.52) is defined as

$$\left| \mathrm{ref}_{421}\left(\quad {}_g \right) \right\rangle = e^{i \ {}_4\left(\quad {}_L \right)} P_4^{fg} e^{\ iH_g t_{42}} P_2^{gf} e^{\ iH_f t_{21}} P_1^{fg} e^{iH_g t_{31}} \left| \quad {}_g \right\rangle, \tag{3.54}$$

and arises when the first pulse creates a nuclear wave packet on the f surface that propagates until the second pulse transfers the amplitude back to g. There the wave packet evolves until the fourth pulse induces the final excitation back to f. Preparation of the target and reference states correspond with the illustrations in Fig. 3.4 for $\left| (3)_f \right\rangle$ and $\left| (421)_f \right\rangle$, respectively.

For molecular state reconstruction, the target and reference states are represented using a discrete position basis $\{|x_n\rangle\}$ with a spacing x between elements. Inserting the completeness relation for this discrete set into Eq. (3.52) yields

$$z_m = \sum_{n=0}^{N} x \left\langle \mathrm{ref}_{421}\left(\quad {}_g \right) \middle| x_n \right\rangle \left\langle x_n \middle| \mathrm{tar}_3\left(\quad {}_g \right) \right\rangle, \tag{3.55}$$

or, for a collection of M measurements,

$$\mathbf{z} = \mathbf{R}\mathbf{t}\,, \tag{3.56}$$

where the signal vector is defined by Eq. (3.51) , the reference matrix is defined by

$$R_{mn} = \left\langle \mathrm{ref}_{421}\left(\quad {}_g \right) \middle| x_n \right\rangle \quad x\,, \tag{3.57}$$

and the target vector is defined as

$$t_n = \left\langle x_n \middle| \mathrm{tar}_3\left(\quad {}_g \right) \right\rangle. \tag{3.58}$$

The elements of the target vector, which are presumedly unknown, are determined by numerically inverting Eq. (3.56) using singular value decomposition (SVD) of the reference matrix. The SVD of **R** is[11]

$$\mathbf{R} = \mathbf{U}\mathbf{W}\mathbf{V}^{\dagger} \tag{3.59}$$

where **V** is an $N \quad N$ unitary matrix, **U** is an $M \quad N$ row unitary matrix, and **W** is an $N \quad N$ diagonal matrix with singular values $W_{jj} \quad 0$. An inverse of **R** is not defined if any of the singular values are zero, as the inverse of **W** is then not defined. But a pseudo-inverse of **R** can be constructed from its SVD as

$$\mathbf{R}_T^{\ 1} = \mathbf{V}\mathbf{W}_T^{\ 1}\mathbf{U}^{\dagger}\,, \tag{3.60}$$

where the modified inverse of **W** is defined as

$$\left(\mathbf{W}_T^{\ 1}\right)_{jj} = \begin{matrix} 1/W_{jj} & \text{if } W_{jj}/W_{\max} > T \\ 0 & \text{otherwise} \end{matrix} . \tag{3.61}$$

In Eqs. (3.60) and (3.61), the tolerance T is a numerical parameter to cutoff those singular values which are below a fraction of the maximum singular value $W_{\max}$. Applying the pseudo-inverse to Eq. (3.56) yields the reconstructed vector

$$\mathbf{r} = \mathbf{R}_T^{\ 1}\mathbf{z} \tag{3.62}$$

which for a given value of the tolerance minimizes the norm $|\mathbf{r}|$ and residual $|\mathbf{z} \quad \mathbf{Rr}|$ of all possible solutions.[11] As a measure of the reconstruction accuracy we define the fidelity

$$f = \frac{|\mathbf{r}^{\dagger} \quad \mathbf{t}|}{|\mathbf{r}||\mathbf{t}|}, \tag{3.63}$$

which lies between 0 and 1.

The present formulation of state reconstruction is similar to the approach taken in QSH, but two differences deserve special attention. First, the source of the interference signal in the present case is a nonlinear WPI experiment, while QSH uses linear WPI data. Second, the definitions of the target and reference states are substantially different. Here the target state is a wave packet propagated under H_f, while in QSH the target state does not propagate but remains localized at the vertical transition point. Furthermore, here the reference states are not restricted to a single line through phase space, but rather explore a finite volume defined by the pulse bandwidth and the range of inter-pulse delays. These distinctions give the present method the possibility of reconstructing a much larger class of potential target wave packets.

Like QSH, the present molecular state reconstruction scheme requires detailed knowledge about both the initial and final electronic levels. When such information is available, computational approaches to quantum state determination are viable, if not altogether more practical; the computational requirements to compute the M reference wave packets comprising the reference matrix seem to obviate the need for an experimental state reconstruction under these circumstances. However, as was the case with linear WPI and QSH, an ability to reconstructed the quantum state of a molecule provides new opportunities for performing *experimental quantum chemistry*, where now transient wave forms of reacting species are potential for wave function imaging.

Model Harmonic System

To discuss in detail the quadrilinear interference terms and their potential use for state reconstruction we first consider a model molecular system with harmonic oscillator surfaces comprising the two electronic levels. The oscillators have the same angular frequency , but different equilibrium configurations. For the initial electronic level we take

$$H_g = \frac{p^2}{2} + \frac{{}^2}{2} x^2 \tag{3.64}$$

with the mass of the oscillator, p the linear momentum, and x the relative displacement about the equilibrium position. We express H_g in terms of the ladder operator,

$$a = \frac{}{2}^{1/2} \quad x + i\frac{p}{} \quad , \tag{3.65}$$

which obeys the commutation relation

$$a, a^{\dagger} \quad = 1 . \tag{3.66}$$

Hence

$$H_g = \quad a^{\dagger} a + \frac{1}{2} \quad . \tag{3.67}$$

The corresponding energy eigenstates satisfy

$$H_g |n\rangle = E_g(n)|n\rangle , \tag{3.68}$$

for $n = 0,1,2,\ldots$,with

$$E_g(n) = \quad (n + 1/2) . \tag{3.69}$$

the eigenenergy. The *f*-state Hamiltonian is

$$H_f = \frac{p^2}{2} + \frac{}{2}^{2}\left(x \quad x_f\right)^2 + \quad {}_f , \tag{3.70}$$

where x_f is the displacement in equilibrium position relative to *g* and ${}_f$ is the bare electronic-energy difference between *f* and *g*. In Appendix A, we show that using the unitary displacement operator

$$D(\quad) = e^{\quad a^{\dagger} \quad a} , \tag{3.71}$$

where is in general a dimensionless complex number, the *f*-state Hamiltonian can be expressed as

$$H_f = D\left(\quad {}_f\right)\left(H_g + \quad {}_f\right) D^{\dagger}\left(\quad {}_f\right) \tag{3.72}$$

with $_f = (m \quad / 2)^{1/2} x_f$. The *f* energy eigenstates are given by

$$|\bar{n}\rangle = D(\quad _f)|n\rangle \tag{3.73}$$

with corresponding eigenenergies

$$E_f(n) = E_g(n) + \quad _f . \tag{3.74}$$

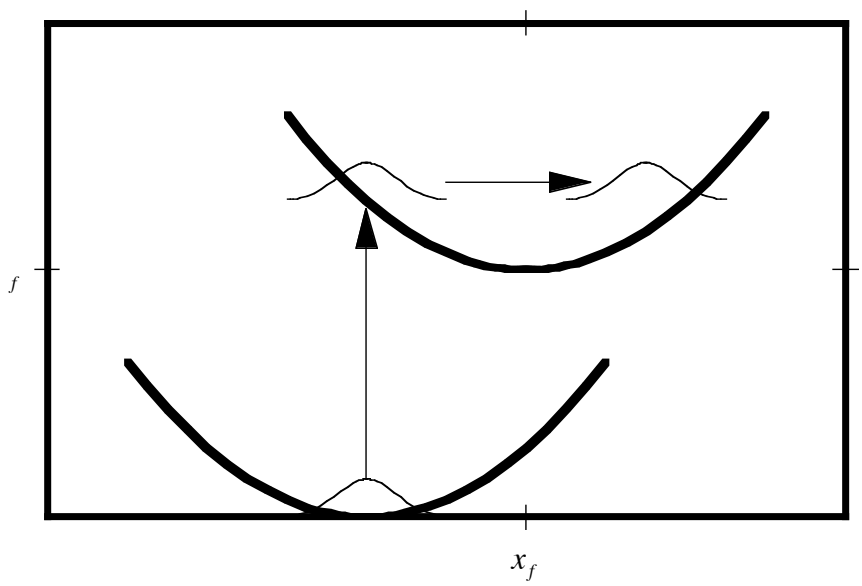

Fig. 3.6 The two harmonic potential surfaces used to describe the model molecule. The final surface has a larger bare electronic energy $_f$ and a larger equilibrium position x_f. The frequency of the oscillators is assumed to be the same. Preparation of a one-pulse wave packet is overlaid.

In our analysis, we specialize to the case that all four pulses are of a sufficiently short duration that any nuclear dynamics occurring during their interaction with the molecule can be neglected. In this impulsive approximation, shaping of the nuclear wave packets due to the effects of finite pulse duration are excluded, but analytical functional forms for the wave packet dynamics can be obtained.

To investigate the impulsive limit, we express the transition amplitude for the pulse propagator in the position eigenbasis as

$$\langle x\,|P_j^{fg}|x\rangle = i\quad d\ \langle x\,|e^{iH_f}\quad {}_{fg}\ \mathbf{e}_j e^{\ iH_g}\ |x\rangle A_j(\ )\cos\quad {}_j(\ ).$$

Owing to the (assumed) ultrashort nature of the temporal envelope, nuclear dynamics that transpire during the pulse interactions are negligible and the latter equation can be reduced to

$$\langle x\,|P_j^{fg}|x\rangle = i\langle x\,|\quad {}_{fg}\ \mathbf{e}_j|x\rangle\Big(d\ e^{i\ {}_f}\ A_j(\ )\cos\quad {}_j(\ ) \tag{3.75}$$

$$= i\quad {}_{fg}(x)\ \mathbf{e}_j\quad {}_j\big(\ {}_f\big)e^{\ i\ {}_j(\ {}_f)}\ (x\quad x),$$

where (x) is the Dirac delta function. By neglecting the coordinate dependence of the transition dipole-moment function the pulse propagator reduces in the impulsive approximation to the constant

$$P_j^{fg} = i\quad {}_{fg}\quad {}_j e^{\ i\ {}_j}, \tag{3.76}$$

where ${}_j = \ {}_j\big(\ {}_f\big)$, ${}_j = \ {}_j\big(\ {}_f\big)$ and ${}_{fg} = \ {}_{fg}\ \mathbf{e}_j$. Note that that the validity of the impulsive approximation results from general considerations about the brevity of the pulses with respect to the nuclear dynamics and is independent of the harmonic model.

In the impulsive approximation, we can write down the form of the wave packets prepared on the harmonic *f* surface. With the help of the results in Appendix A, we find the one-pulse wave packets given in Eqs. (3.27) to (3.30) can be written as

$$\big|(1)_f\big\rangle = i\quad {}_{fg}\quad {}_1 e^{\ i\left(\ {}_1 + E_f(n)t_{41}\right)\ i\ {}_f^2 \sin\ t_{41}} D\Big(\ {}_f\big(1\quad e^{\ i\ t_{41}}\big)\Big)|n\rangle \tag{3.77}$$

$$\left|(2)_f\right\rangle = i \quad {}_{fg} \quad {}_2 e^{i\left({}_2 + E_f(n) t_{42}\right)} \; i \; {}_f^2 \sin \quad t_{42} D\left(\quad {}_f \left(1 \quad e^{i \quad t_{42}}\right)\right)\left|n\right\rangle \tag{3.78}$$

$$\left|(3)_f\right\rangle = i \quad {}_{fg} \quad {}_3 e^{i\left({}_3 + E_f(n) t_{43}\right)} \; i \; {}_f^2 \sin \quad t_{43} D\left(\quad {}_f \left(1 \quad e^{i \quad t_{43}}\right)\right)\left|n\right\rangle \tag{3.79}$$

$$\left|(4)_f\right\rangle = i \quad {}_{fg} \quad {}_4 e^{i \; {}_4} \left|n\right\rangle \tag{3.80}$$

while the three-pulse wave packets in Eqs. (3.31) to (3.34) are

$$\left|(421)_f\right\rangle = \quad i \quad {}_{fg}^{3} \quad {}_4 \quad {}_2 \quad {}_1 e^{i\left({}_L \quad E_f(n)\right) t_{21}} \; i \; {}_4 \; i \; {}_f^2 \sin \quad t_{21} \tag{3.81}$$

$$D\left(\quad {}_f \left(1 \quad e^{i \quad t_{21}}\right) e^{i \quad t_{42}}\right)\left|n\right\rangle$$

$$\left|(321)_f\right\rangle = \quad i \quad {}_{fg}^{3} \quad {}_3 \quad {}_2 \quad {}_1 e^{i\left({}_L \quad E_f(n)\right) t_{21}} \; i \; {}_3 \; i \; {}_f^2 \left(\sin \quad t_{21} + \sin \quad t_{31} \quad \sin \quad t_{32}\right) \tag{3.82}$$

$$D\left(\quad {}_f \left(\left(1 \quad e^{i \quad t_{21}}\right) e^{i \quad t_{32}} \quad 1\right) e^{i \quad t_{43}} + \quad {}_f\right)\left|n\right\rangle$$

$$\left|(431)_f\right\rangle = \quad i \quad {}_{fg}^{3} \quad {}_4 \quad {}_3 \quad {}_1 e^{i\left({}_1 + \quad {}_L t_{43} + \quad {}_f t_{31}\right)} \; i \; {}_f^2 \sin \quad t_{31} \tag{3.83}$$

$$D\left(\quad {}_f \left(1 \quad e^{i \quad t_{31}}\right) e^{i \quad t_{43}}\right)\left|n\right\rangle$$

$$\left|(432)_f\right\rangle = \quad i \quad {}_{fg}^{3} \quad {}_4 \quad {}_3 \quad {}_2 e^{i\left({}_2 + \quad {}_L t_{43} + \quad {}_f t_{32}\right)} \; i \; {}_f^2 \sin \quad t_{32} \tag{3.84}$$

$$D\left(\quad {}_f \left(1 \quad e^{i \quad t_{32}}\right) e^{i \quad t_{43}}\right)\left|n\right\rangle$$

We calculate the quadrilinear overlaps arising from the wave packets in Eqs. (3.77) to (3.84) for the case $n = 0$ and find

$$\left\langle (432)_f \middle| (1)_f \right\rangle = \quad {}_{fg}^{4} \quad {}_4 \quad {}_2 \quad {}_3 \quad {}_4 e^{i\left({}_L \quad {}_f\right) t_{43} + i\left({}_L \quad {}_f\right) t_{21}} \tag{3.85}$$

$$\exp \quad {}_f^2 \left(e^{i \quad t_{21}} + e^{i \quad t_{32}} + e^{i \quad t_{43}} + e^{i \quad t_{41}} \quad e^{i \quad t_{31}} \quad e^{i \quad t_{42}} \quad 2\right)($$

$$\left\langle (431)_f \middle| (2)_f \right\rangle = \quad {}_{fg}^{4} \quad {}_4 \quad {}_2 \quad {}_3 \quad {}_4 e^{i\left({}_L \quad {}_f\right) t_{43} \; i\left({}_L \quad {}_f\right) t_{21}} \tag{3.86}$$

$$\exp \quad {}^{2}_{f}\left(e^{i\ t_{21}} \quad e^{\ i\ t_{32}} + e^{i\ t_{43}} \quad e^{i\ t_{41}} + e^{i\ t_{31}} + e^{\ i\ t_{42}} \quad 2\right)($$

$$\left\langle (421)_f \middle| (3)_f \right\rangle = \quad {}^{4}_{fg} \quad {}_{4} \quad {}_{2} \quad {}_{3} \quad {}_{4} e^{i(\ {}_{L} \quad {}_{f})t_{43} \ i(\ {}_{L} \quad {}_{f})t_{21}} \qquad \text{-(3.87)}$$

$$\exp \quad {}^{2}_{f}\left(e^{i\ t_{21}} \quad e^{i\ t_{32}} + e^{\ i\ t_{43}} \quad e^{i\ t_{41}} + e^{i\ t_{31}} + e^{i\ t_{42}} \quad 2\right)($$

$$\left\langle (321)_f \middle| (4)_f \right\rangle = \quad {}^{4}_{fg} \quad {}_{4} \quad {}_{2} \quad {}_{3} \quad {}_{4} e^{\ i(\ {}_{L} \quad {}_{f})t_{43} \ i(\ {}_{L} \quad {}_{f})t_{21}} \qquad (3.88)$$

$$\exp \quad {}^{2}_{f}\left(e^{i\ t_{21}} + e^{i\ t_{32}} + e^{i\ t_{43}} + e^{i\ t_{41}} \quad e^{i\ t_{31}} \quad e^{i\ t_{42}} \quad 2\right)($$

In Figs. 3.7 to 3.10 we plot Eqs. (3.85) to (3.88), respectively, for the case ${}^{2}_{f} = 2$ and ${}_{L} = \quad = {}^{2}_{f} \quad + \quad {}_{f}$ with $t_{43} = 0.25$, where is the vibrational period. These contour plots use solid (dashed) lines to denote positive (negative) values with these lines spaced by one-tenth of the signal maximum ${}^{4}_{fg} \quad {}_{1} \quad {}_{2} \quad {}_{3} \quad {}_{4}$. In the upper panel of each figure we plot the magnitude of the overlap, in the middle the real component, and in the bottom panel the imaginary component. For the harmonic system the complex signal is repetitive along the t_{32} axis. Periodicity along the other time axis, t_{21}, depends on the value of the locking frequency ${}_{L}$ and its offset from resonance with the vertical electronic difference energy. A similar effect has been observed in linear WPI experiments; see Ref. [1].

The sum of Eq. (3.85) and the conjugate of Eq. (3.88) comprises the interference $p_{1,1}$; recall Eq. (3.41). From Figs. 3.7 and 3.10 we see that the form of these two overlaps is very different, but that they both have maxima for the same values of inter-pulse delays.

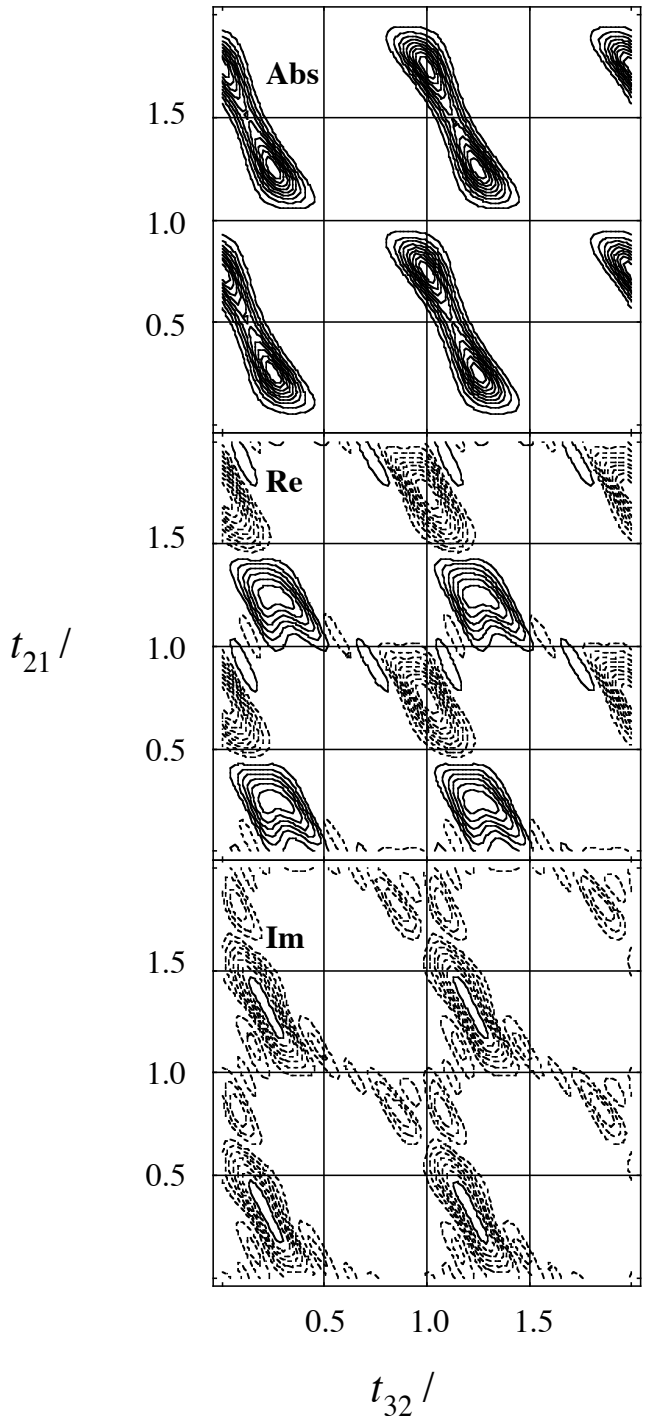

Fig. 3.7 One-color $\langle (432)_f | (1)_f \rangle$ contribution for a model harmonic system.

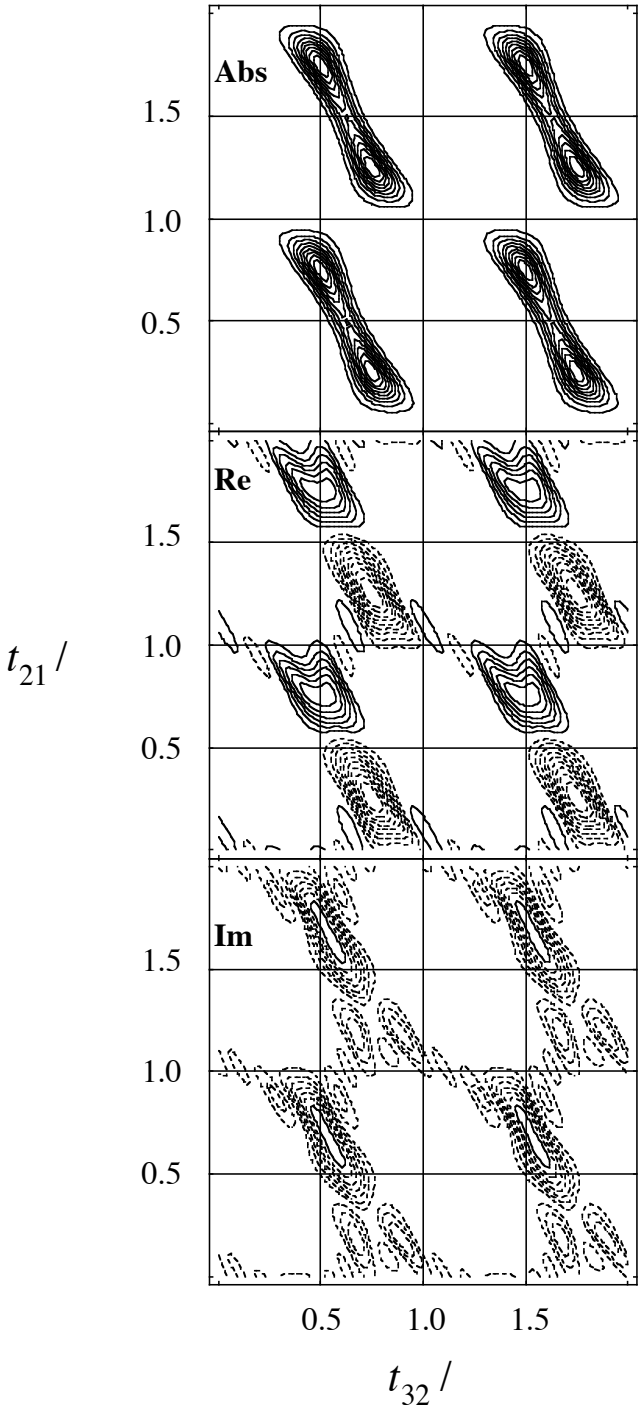

Fig. 3.8 One-color $\langle (431)_f | (2)_f \rangle$ contributions for a model harmonic system.

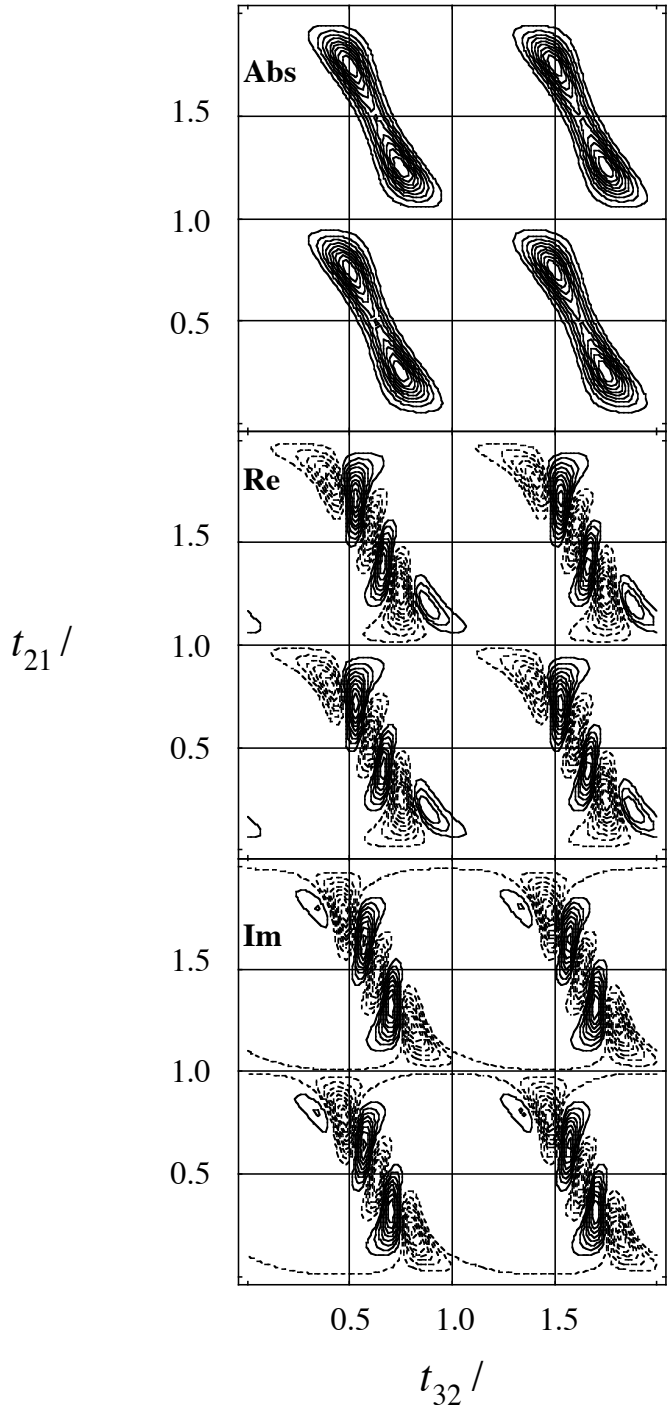

Fig. 3.9 One-color $\langle (421)_f | (3)_f \rangle$ contributions for a model harmonic system.

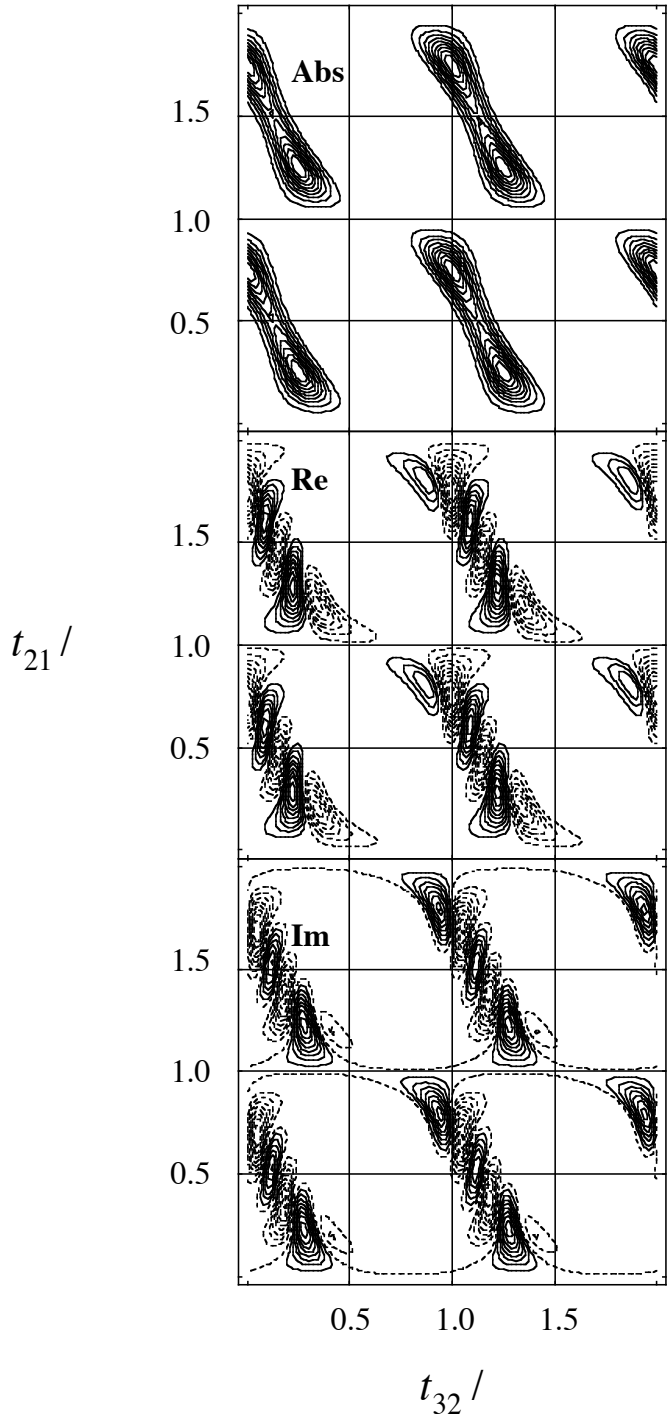

Fig. 3.10 One-color $\langle (321)_f | (4)_f \rangle$ contributions for a model harmonic system.

Indeed, the magnitude of $\left\langle (432)_f \middle| (1)_f \right\rangle$ and $\left\langle (321)_f \middle| (4)_f \right\rangle$ are the same at arbitrary values of (t_{21}, t_{32}, t_{43}), while the phases of these overlaps are generally different. Likewise, the sum of Eqs. (3.86) and (3.87) comprises the interference $p_{1,1}$, as given in Eq. (3.42). From Figs. 3.7 and 3.10, it is apparent that $p_{1,1}$ and $p_{1,1}$ have maxima for the same values of interpulse delays. This is not due to the specific choice of $t_{43} = 0.25$, but is rather a consequence of the harmonic oscillations. A single quadrilinear overlap is not isolable, and molecular state reconstruction is not possible.

To rationalize how coincidences in magnitude are determined by the harmonic motion of the vibrations we use phase-space diagrams to trace the motion of each wave packet leading to maximal overlap. This is facilitated by the quasi-classical nature of a coherent state, whose "trajectory", i.e. time-dependent average of position and momentum, matches that of the corresponding classical system. For $\left\langle (432)_f \middle| (1)_f \right\rangle$ and $\left\langle (321)_f \middle| (4)_f \right\rangle$ a maximum in the overlap occurs for $t_{21} = t_{32} = 0.25$ and in Figs. 3.11 and 3.12 we plot the trajectory for each of these wave packets in phase space. From Figs. 3.11 and 3.12 it is apparent that the dynamics leading to a maximum in each contribution are different. Similar plots give insight into the common maxima of the $\left\langle (431)_f \middle| (2)_f \right\rangle$ and $\left\langle (421)_f \middle| (3)_f \right\rangle$ overlaps, e.g., at $t_{21} = t_{43} = 0.25$ and $t_{32} = 0.75$.

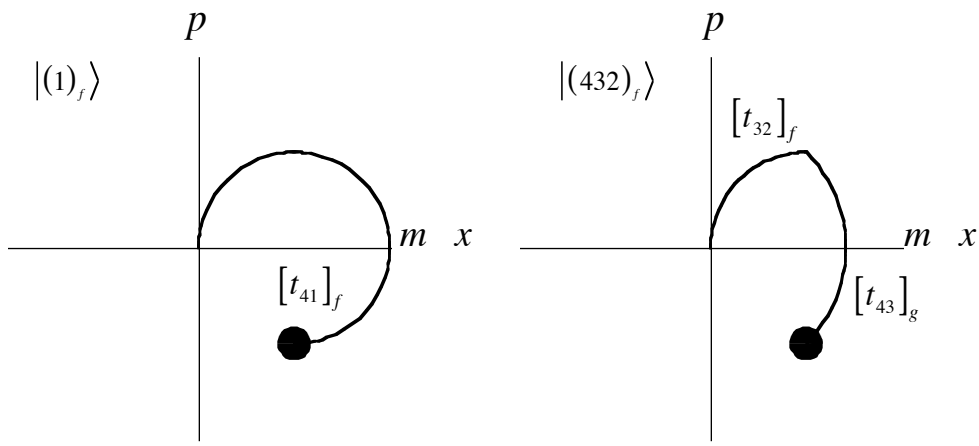

Fig. 3.11 Phase-space trajectory diagrams for $|(1)_f\rangle$ and $|(432)_f\rangle$ wave packets which lead to maximal coincidence in wave packet overlap. Brackets denote time-evolution for the enclosed amount of time and the solid circle represents the end point of the trajectory. In the figure, $t_{21} = t_{32} = t_{43} = 0.25$.

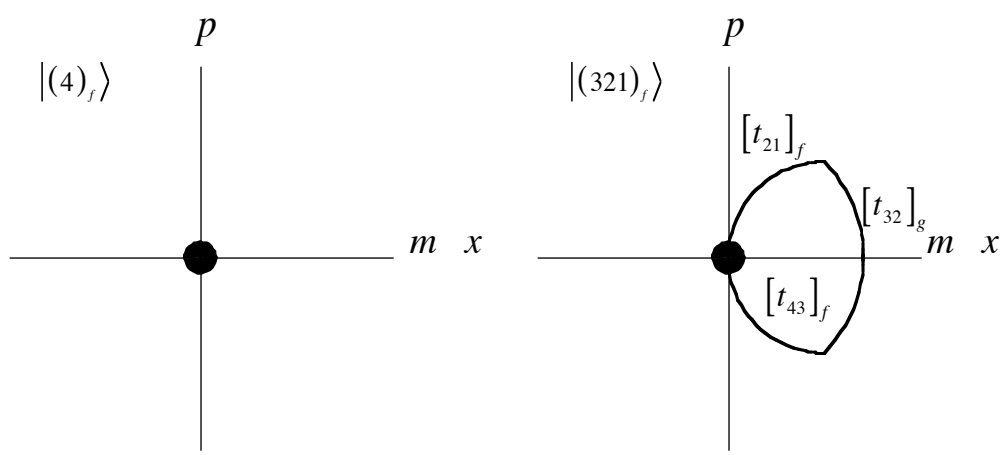

Fig. 3.12 Phase-space trajectory diagrams for $|(4)_f\rangle$ and $|(321)_f\rangle$ wave packets which lead to maximal coincidence in wave packet overlap. Brackets denote time-evolution for the enclosed amount of time and the solid circle represents the end point of the trajectory. In the figure, $t_{21} = t_{32} = t_{43} = 0.25$.

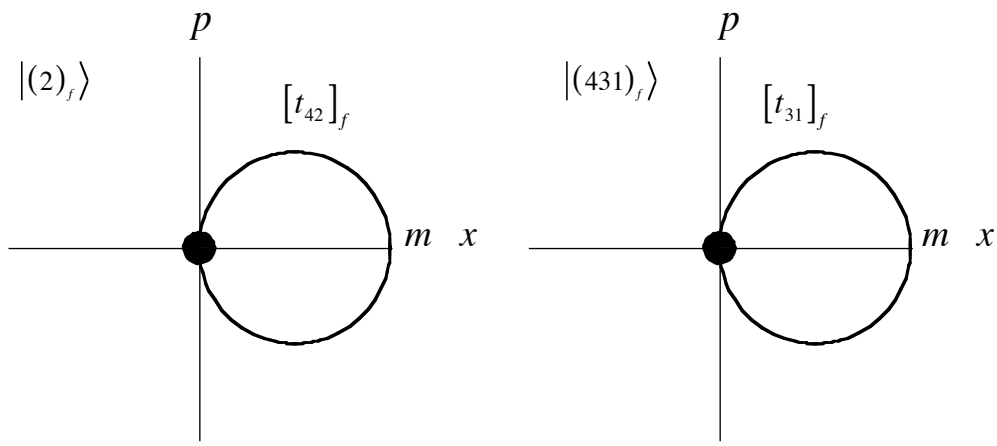

Fig. 3.13 Phase-space trajectory diagrams for $|(2)_f\rangle$ and $|(431)_f\rangle$ wave packets which lead to maximal coincidence in wave packet overlap. Brackets denote time-evolution for the enclosed amount of time and the solid circle represents the end point of the trajectory. In the figure, $t_{21} = t_{43} = 0.25$ and $t_{32} = 0.75$.

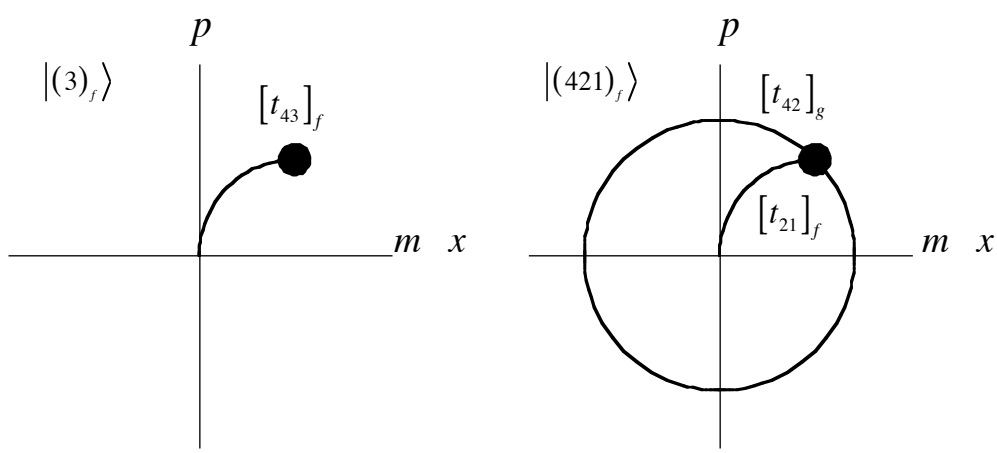

Fig. 3.14 Phase-space trajectory diagrams for $|(3)_f\rangle$ and $|(421)_f\rangle$ wave packets which lead to maximal coincidence in wave packet overlap. Brackets denote time-evolution for the enclosed amount of time and the solid circle represents the end point of the trajectory. In the figure, $t_{21} = t_{43} = 0.25$ and $t_{32} = 0.75$.

Model Photodissociative System

The model harmonic system is useful for gaining insight into the wave packets prepared in a one-color nonlinear WPI experiment, but does not lend itself to an implementation of molecular state reconstruction; in the foregoing discussion we found the contributions to the interference signal have maxima for the same values of interpulse delay. Such coincidences in wave-packet dynamics prevent the means to diminish mixing of overlap information using spectral discrimination with the pulse bandwidths. But for the case of a model photodissociative system, in which the excited-electronic level is an exponentially decaying function of position, wave packet overlaps can be minimized through control of the interpulse delays.

We take the initial Hamiltonian to be harmonic, as in Eq. (3.64). The final-state Hamiltonian is

$$H_f = \frac{p^2}{2} + De^{\quad x} + \quad {}_f \tag{3.89}$$

where D is the Franck-Condon energy (relative to the bare electronic-difference energy ${}_f$) and is an inverse length scale which controls how the potential decays. To determine the interferogram for this system we use numerical calculations. We take numerical values of $= 63.5$ amu, $= 2\ c\left(250\ \text{cm}^{-1}\right)$, $D = 2\ c\left(1000\ \text{cm}^{-1}\right)$, and $= 10.85\ \text{Å}^{-1}$. A plot of the potential surfaces is shown in Fig. 3.15. While the parameters are suggestive of diatomic iodine, the present potential only serves as models for the investigation of photo-dissociative dynamics. Both locking frequencies are resonant with the vertical transition energy ${}_L = \quad {}_L = D + \quad {}_f$.

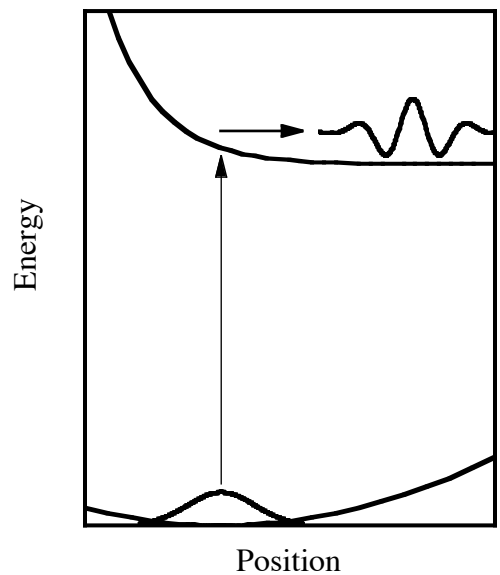

Fig. 3.15 The model dissociative potential used in the simulation. Wave packets are prepared by vertical excitation using one of the pulses and then begin to dissociate. For the three-pulse wave packet dissociation is halted by a de-excitation back to the harmonic ground state, while the one-pulse wave packets may continue dissociating.

We numerically calculate the wave packets in Eqs. (3.27) to (3.30) by representing them over a position grid.[12] Invoking the impulsive approximation for the pulses, we require only the action of the time-evolution operator in each electronic level which we approximate using a split-propagation operator with fast Fourier transforms between position and momentum space operations.[13] We use a propagation step of 0.01 fs. Setting $t_{43} = 33.35$ fs, which is approximately a quarter of the ground state vibrational period $_{\text{vib}} = 133.35$ fs, we scan t_{21} and t_{32} each from 0 to $_{\text{vib}}$ in 50 equally spaced steps. Overlaps are then calculated between the wave packets. In Fig. 3.16, we show the quadrilinear interference $p_{1,1}$.

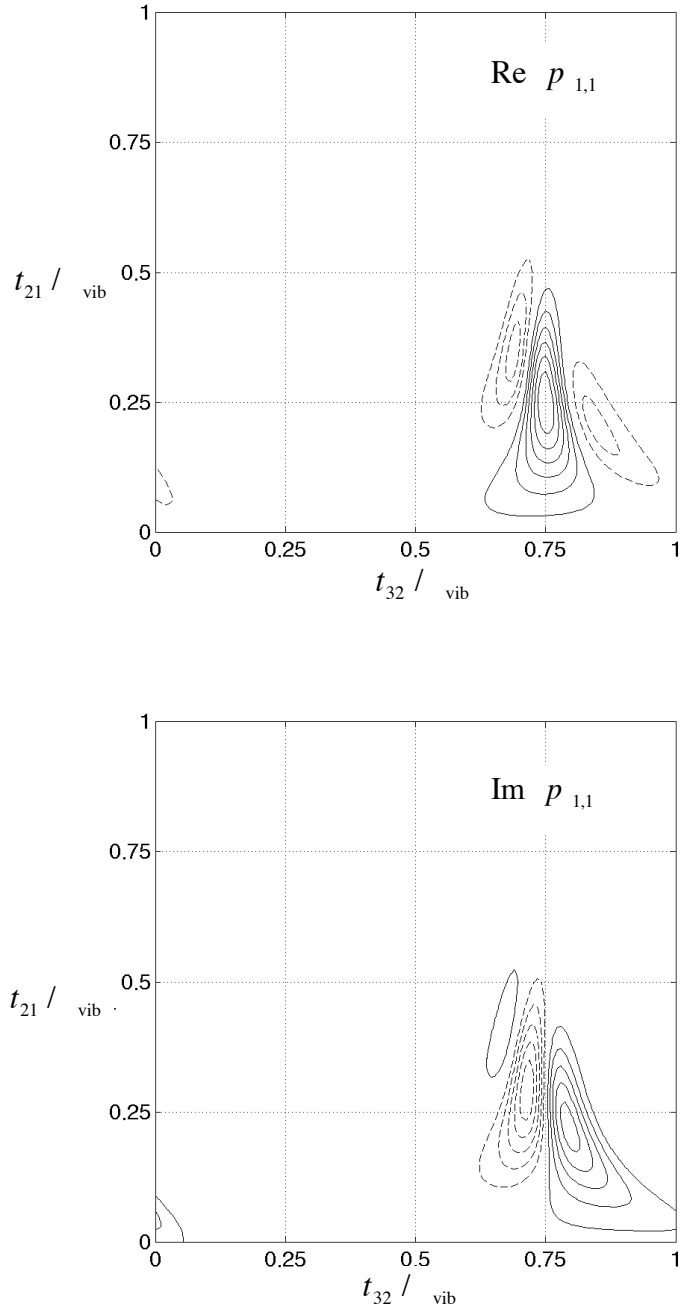

Fig. 3.16. The real and imaginary components of $p_{1,1}$ for a model photodissociative system. Solid (dashed) lines denote positive (negative) values of the interference in units of 1/7th the signal maximum $^{2}_{fg}$ 1 2 3 4. Here t_{43} = 0.25 vib = 33.35 fs .

The large features in Fig. 3.16 residing in the lower right quadrant of each contour plot is the interference due to $\left\langle (421)_f \middle| (3)_f \right\rangle$. The small features located near the $(0,0)$ point in the interferogram are due to $\left\langle (431)_f \middle| (2)_f \right\rangle$. The latter contribution to the interference decays very rapidly as either delay is increased; in both cases the one-pulse wave packet $\left| (2)_f \right\rangle$ propagates further down the dissociative potential. The same can be said for the three-pulse wave packet $\left| (431)_f \right\rangle$, but it spends a quarter of a vibrational cycle on the g surface, so that as the amplitude of the initial wave packet motion is increased, the end point of the phase-space trajectory is continuously moved further from the target state. In contrast, the $\left\langle (421)_f \middle| (3)_f \right\rangle$ repeats along the t_{32} axis with a periodicity given by the harmonic period of g. This results from the harmonic motion of the three-pulse wave packet during this delay. After peaking at $t_{21} = t_{43}$, the overlap decays along the t_{21} axis. The peak arises from maximal coincidence between the wave packets, as was the case for the model harmonic system, but as the three-pulse wave packet spends more time in the excited electronic level it too begins to dissociate.

Due to the dynamical discrimination resulting from the dissociative potential, the interferogram supplies the information necessary for reconstruction of the target state defined in Eq. (3.53). Using the calculated interferogram in Fig. 3.16 and the reference states in Eq. (3.54), we solve the matrix equation given by Eq. (3.56) for the model dissociative system. The results of the reconstruction procedure are shown in Fig. 3.17, where a fidelity of 1.000 (to within machine precision) was obtained.

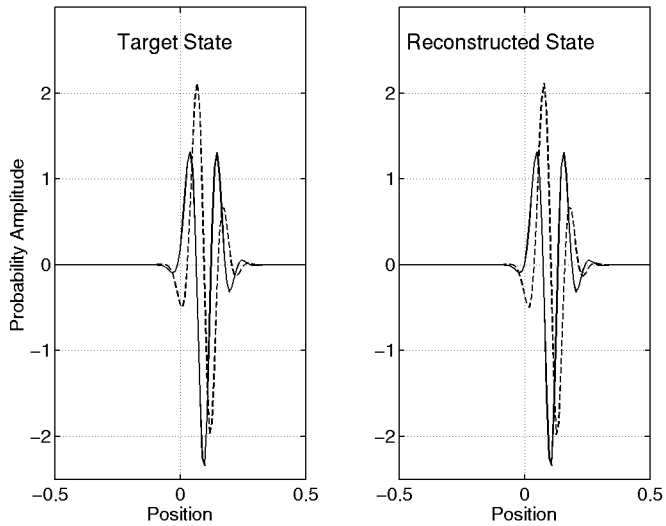

Fig. 3.17 The target and reconstructed states for the dissociative system. The solid (dashed) lines are the real (imaginary) components of the wave function. Position is measured in angstroms (Å), probability amplitude is measured in units of $Å^{-1/2}$. The magnitude of the overlap between these normalized wave packets is unity to within machine precision.

Remarks

In this chapter we have formulated the theory of one-color nonlinear WPI and simulated its application to model harmonic and photodissociative systems. In the case of the former, analytic expressions of the wave packet dynamics were obtained but molecular state reconstruction was not possible given substantial mixing of the two contributing overlaps. For the case of a dissociative system, one of the interference contributions was diminished due to the dynamics of the model molecular Hamiltonian. Consequently, the information needed to implement state reconstruction was available from the calculated interferogram and an application of the state reconstruction scheme outlined in this chapter yielded a reconstructed state with unit fidelity. These simulations

demonstrated the concept of a one-color reconstruction technique and highlighted some aspects of signal isolation which will benefit future experimental investigations. Though our investigations have been for systems with a single vibrational degree of freedom, Cina has noted that the prospects for a successful one-color state reconstruction also extend to bound multimode systems, where long propagation times in an excited electronic level could diminish the mixing of wave-packet overlaps as a result of incommensurate vibrational periods.[4]

A one-color reconstruction technique necessitates information about the final-state Hamiltonian to calculate the reference wave packets. The availability of such information raises the question as to whether a one-color experimental state reconstruction scheme is practical or even necessary; if the three-pulse reference states can be calculated, why not the one-pulse target state? There are several reasons motivating implementation of a one-color reconstruction technique. First, as noted shown by Bucksbaum and coworkers using a variation of quantum state holography,[14] state reconstruction can drive adaptive pulse-shaping experiments, be they closed-loop or otherwise. This suggests that one could investigate excited-state molecular dynamics by using molecular state reconstruction to tailor specific initial nuclear states. The advantages afforded by using nonlinear WPI now extends the same degree of control to the reconstruction and shaping of transient wave packets in a photochemical reaction. Such aspects are also important to molecular applications of quantum computing, where one-color state reconstruction could be useful for performing read-out operations on molecular computers running, for example, quantum simulation algorithms.[15]

Second, knowledge of an excited-state nuclear Hamiltonian will realistically be incomplete. Though the potential underlying nuclear dynamics may be well-characterized near the vertical transition point and in small regions thereabouts, information about the potential surface far from equilibrium is generally more difficult to gain; computationally there are limits on the resources and techniques which one uses to solve the electronic Schrödinger equation. As calculations of the reference states are restricted to those molecular conformations for which the potential is known, there are often a wide range of nuclear motions which can not be calculated. But such a limitation is not placed on the target state, whose dynamics are determined by the actual Hamiltonian, known only to the molecule.

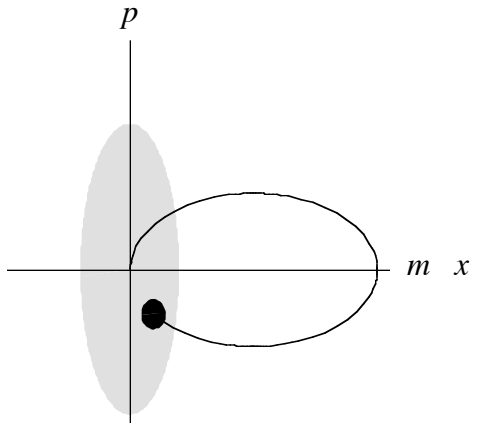

Fig. 3.18. A target state returns after undergoing large amplitude motion. The shaped area represents the region of phase space in which reference states can be calculated.

The target state is free to explore “unknown” regions of phase space, i.e. regions of phase-space for which reference states cannot be calculated. If the target state were to return from these large amplitude explorations to the known regions of phase space, the one-color reconstruction technique could then be used to detect the subsequent changes in the target state. An example of the latter case is a pre-dissociative system, for which a

dissociating wave packet is partially reflected by finite a potential barrier back to the Franck-Condon point. In Fig. 3.18, we shade the region of known phase space and trace the bound trajectory of the target state. After visiting the outer turning point, a target state that returns to the known region of phase space could be reconstructed.

Notes

1. N. F. Scherer, R. J. Carlson, A. Matro, M. Du, A. J. Ruggiero, V. Romero-Rochín, J. A. Cina, G. R. Fleming, and S. A. Rice, J. Chem. Phys. **95**, 1487 (1991).

2. N. F. Scherer, A. Matro, L. D. Ziegler, M. Du, R. J. Carlson, J. A. Cina, and G. R. Fleming, J. Chem. Phys. **96**, 4180 (1992).

3. J. A. Cina and R. A. Harris, J. Chem. Phys. **100**, 2531 (1994).

4. J. A. Cina, J. Chem. Phys. **113**, 9488 (2000).

5. P. Tian, D. Keusters, Y. Suzaki, and W.S. Warren, Science **300**, 1533 (2003).

6. C. Leichtle, W. P. Schleich, I. Sh. Averbukh, and M. Shapiro, Phys. Rev. Lett. **80**, 1418 (1998).

7. I. Sh. Averbukh, M. Shapiro, C. Leichtle, and W. P. Schleich, Phys. Rev. A **59**, 2163 (1999).

8. V. Blanchet, C. Nicole, M.-A. Bouchene, and B. Girard, Phys. Rev. Lett. **78**, 2716 (1997).

9. M. A. Bouchene, C. Nicole, and B. Girard, J. Phys. B: At. Mol. Opt. Phys. **32**, 5167 (1999).

10. G. P. Tolstov, *Fourier Series* (Dover Publications Inc., New Jersey, 1976).

11. W. H. Press, S. A. Teukolsky, W. T. Vetterling, and B. P. Flannery, *Numerical Recipes in C* (Cambridge University Press, Cambridge, 1988).

12. As the potential is dissociative, the range of the grid needed to accurately propagate the wave packets is determined, in part, by the delays used. For the $|(1)_f\rangle$ and $|(2)_f\rangle$ wave packets, a grid of 2098 equally spaced points from –3.5 Å to 11.5 Å was necessary to prevent artificial reflection due to the boundary conditions. The wave packets $|(3)_f\rangle$ and $|(4)_f\rangle$ explored a smaller spatial region and a grid from –0.5 Å to 3.5 Å was used. The momentum gained through dissociating required a smaller grid spacing be used for the first pair of wave packets.

13. M. D. Feit, J. A. Fleck Jr., and A. Steiger, J. Comp. Phys. **47**, 412 (1982).

14. T. C. Weinacht, J. Ahn, and P. H. Bucksbaum, Nature **397**, 233 (1999).

15. M. A. Nielsen and I. L Chuang, *Quantum Computation and Quantum Information* (Cambridge University Press, Cambridge, 2000).